Available online at www.sciencedirect.com

ScienceDirect

Energy Procedia 98 (2016) 30 – 39

Energy Procedia

6th Workshop on Metallization and Interconnection for Crystalline Silicon Solar Cells, 2016

Front metal finger inhomogeneity: its influence on optimization and on the cell efficiency distribution in production lines

Y. Chen[a], Y. Yang[a], W. Deng[a], A. Ali[b], P.J. Verlinden[a], P.P. Altermatt[a]*

[a] *State Key Laboratory for PV Science and Technology, Trina Solar, Changzhou, Jiangsu Province, 213031, P.R. China*
[b]*Department of Physics, Government College University Faisalabad, 38000 Faisalabad, Pakistan*

Abstract

A model is developed for simulating the inhomogeneity of front metal fingers and its influence on the performance of mass-produced crystalline silicon solar cells. First, it is shown by numerical device simulations that, in modern cell design, the optimal number of fingers will be increasingly determined by the emitter sheet resistivity and to a lesser extent by other geometries of the metallization (such as finger width, their cross-sectional area *A*, and the number of bus bars). An example from production shows that the relationship between finger width and the amount of screen-printing paste can be inferred from the data cloud containing short-circuit current and fill factor values of fabricated cells. A logistic function is introduced to fit a broad range of cross-sectional finger shapes. With all this as input, spice simulations are preformed to elucidate the dynamics of cell efficiency in dependency of cross-sectional finger area *A*. The model for finger inhomogeneity is illustrated with a failure analysis. Then, it is shown that finger inhomogeneity contributes only to a small extent to the observed variations in mass production, so the metal fingers can be designed with considerably smaller *A* to save silver without causing a too large spread in efficiency. Finally, a desirable near-future target of $A \approx 300\ \mu m^2$ is derived from a combination of modeling and a literature collection of metallization data. It will not be necessary in future cell design to increase the number of fingers beyond about 155 (equivalent to a finger pitch of about 1 mm), regardless of the number of bus bars or of a multi-bus bar design. Comparing the simulations with the trend in literature data suggests that screen-printing will be the moving target in metallization for some time to come. Mainly economic pain due to high silver prices may favor a transition to (near) silver-free printing techniques.

Peer-review under responsibility of the organizing committee of the Metallization Workshop 2016

Keywords: Silicon solar cells; device simulation; metallization;screen-printing; silver

* Corresponding author. Tel.: +86-519-8158-7679.
E-mail address: pietro.altermatt@trinasolar.com

Peer-review under responsibility of the organizing committee of the Metallization Workshop 2016
doi:10.1016/j.egypro.2016.10.078

1. Introduction

The optimization of the front metal grid influences mainly the short-circuit current density J_{sc} and the fill factor *FF* of the current-voltage (IV) curve of solar cells due to the well-known offset between shading and resistive losses. The open-circuit voltage V_{oc} may be influenced only in cases where the amount of recombination at the front metal contacts varies with grid optimization and if it contributes significantly to the total recombination losses of the cell. It is well known that these IV parameters may also be affected by other parts of the cell than by the front metallization. For example J_{sc} may vary in cell production due to variations in the passivation of the front surface [1], while *FF* may vary due to Si/metal contact resistivity or a variable amount of oxygen and of boron-oxygen (B-O) recombination centers, which cause an injection-dependent and hence a voltage-dependent lifetime. In this paper, we only take variations due to the front metallization into account.

A detailed paper treating inhomogeneity within the front metal grid is the recent one by Wong et al. [2], using the GRIDDLER model. Another paper in the awareness of the authors is Ref. [3]. In our work, the inhomogeneity of the front metal fingers is treated with a SPICE model, which has an IV curve from a numerical device model as input. The paper emphasizes on the caused distribution of J_{sc} and *FF* in mass production and on consequences on metallization and cell design in near future.

Nomenclature

A	Cross-sectional area of a metal finger [μm^2].
a	Curvature factor used in the fitting of cross-sectional finger shapes with Eq. (1).
F	Filling factor of the finger, i.e. A divided by the rectangle spanned by the finger width and finger height.
f	Fractional parameter for quantifying variations of A relative to a fixed A_0, $A = fA_0$.
N	Number of metal fingers on a 156×156 mm^2 large cell.
$R_{s.int}$	Internal lumped series resistance of the cell [Ωcm^2], including Si/metal contact resistance.
$R_{s.seg}$	Resistance [Ω] of a finger segment represented by a resistor in the SPICE simulation.
w_{min}	Minimal width [μm] of metal fingers when printed with hardly any paste, as indicated in Fig. 2

2. Optimal number of fingers

The bases of this paper are two and three dimensional numerical simulations of the semiconductor part of monocrystalline silicon solar cells. The simulations are performed with the software SENTAURUS DEVICE using the silicon parameters of Ref. [4] including an update in the model for the Al-alloyed back surface field (BSF) [5] and for Auger recombination [6]. We choose an advanced cell design for standard production. Without metallization, the cell has a J_{sc} = 40 mA/cm^2 due to a typical nitride antireflection coating, and the cell efficiency is adjusted to 21% by choosing a good selective emitter, leading to both a V_{oc} = 640 mV and a rather high internal lumped series resistance $R_{s.int}$. See Fig. 1 for the simulation results in dependence of the number of front metal fingers. $R_{s.int}$ varies mainly due to the emitter sheet resistivity, and J_{sc} due to a varying amount of recombination in the emitter because the width of its highly-doped n^{++} part is kept constant at 200 µm to accommodate alignment tolerances. Further details of the semiconductor part of the cell are irrelevant to our metallization study and are not given here.

With adding the metallization, J_{sc} becomes approximately 38 mA/cm^2 and cell efficiency is 20%, as is expected from standard cells in 2018 according to the ITRPV roadmap [7]. The fill factor reaches about 80.5% because it is assumed that the B-O complex in the p-type wafer is thoroughly deactivated.

A crucial step in grid optimization is adjusting the number of metal fingers N (or equivalently the finger pitch). It is important to note that in advanced cell designs with a good emitter, the optimum N is mainly imposed by the high emitter sheet resistivity and only to a minor extent by the finger width or other metallization geometries. This has not been the case in cell designs with a low emitter sheet resistivity.

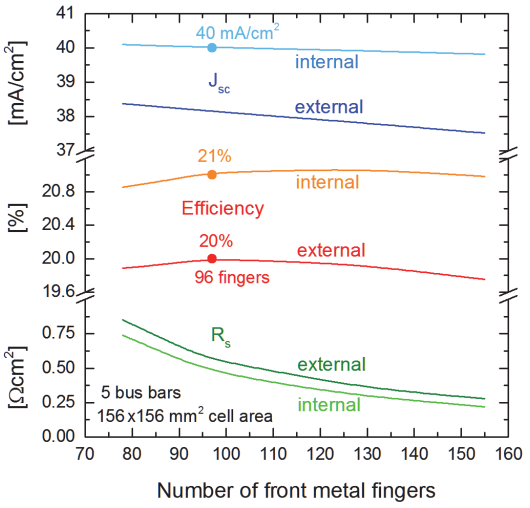

Figure 1. The short-circuit density, cell efficiency and lumped resistance, simulated with SENTAURUS DEVICE, of a hypothetical cell expected in standard mass production in 2018.

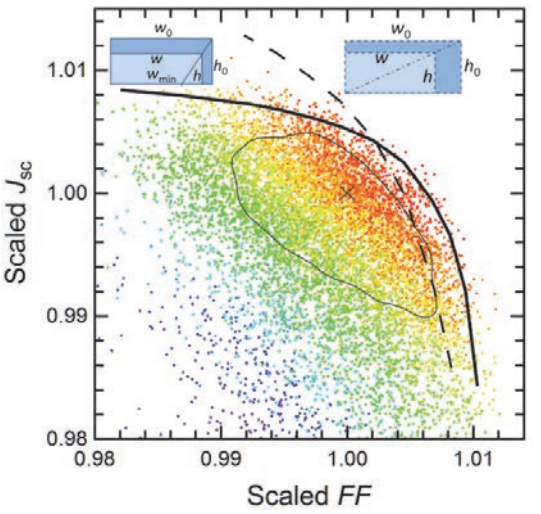

Figure 2. Short-circuit current and fill factor values of 10’000 cells of a failure batch, scaled to the deepest data point, indicated by the cross. Color indicates cell efficiency. The 50% of deepest data points are surrounded by a circle. The fitting of the peripheral cells at the highest efficiency levels (dashed and solid line) are discussed in the text.

3. Variation of finger shape with the amount of printing paste

An important input to our simulations is how the finger shape varies with the amount of screen-printing paste. Or more specifically, how the width w_0 of the fingers depend on the cross-sectional area A. Luckily, this can be inferred from the J_{sc} and *FF* values of fabricated cells. Fig. 2 shows ten thousand J_{sc}, *FF*-points from a failure batch to show the effect boldly (in usual production, the effects are far more subtle). These values are normalized for confidentiality reasons. Our eyes are unable to recognize the density-distribution of such big data clouds and, accordingly, are unable to estimate the median value. Therefore, it is helpful to calculate a bag plot [8] using the software R [9] and the ‘aplpack’ package [10]. A bag plot is a two-dimensional extension of the well-known box plot. In box plots, the median value is the middle point of ranked data. Equivalently, the median value can be obtained by identifying the deepest point in ranked data, i.e. being surrounded by the highest number of ranked data points. The notion of ‘deepest point’ can be extended to two dimensions by the following algorithm: at each data point, an infinite line is attached and rotated. During the rotation, the number of other data points to the left and to the right of the line is counted, respectively. The minimum number is the depth, and the deepest data point is the one where this minimum number is largest. It is usually situated close to the separate median values of the x- and y-components, respectively. The width of the box in the one-dimensional box plot spans 50% of the ranked data situated above and below the median value, and is called the interquartile range (IQR). In the two-dimensional bag plot, the IQR contains 50% of the deepest data points, and is called the bag. In Fig. 2, the deepest data point is plotted as a cross, the 50% of deepest data points are surrounded by a closed line.

To infer how the finger shape varies with the amount of paste, it is useful to consider the peripheral points at the highest efficiency levels because there, all other disturbing variations than the amount of paste are minimized. Varying A with assuming that the width w varies proportionally to A results in the dashed line. This line is calculated in our case with the SPICE model, but it may be calculated without numerical simulations [11] using the analytical equations given in [12] and used in commonly available software such as GRID CALCULATOR [13] or GRIDMASTER [14]. The dashed line obviously does not follow the peripheral points. However, assuming that there is a minimal finger width w_{min}, as indicated in the inset of Fig. 2, the solid line results from the SPICE simulation and describes the peripheral points perfectly. This line also runs in parallel to parts of the bag. The value of w_{min} may be related to the mesh size, but we did not investigate this in more detail.

Having w_{min} extracted from the fabricated data cloud, we now need to describe the dependence of the finger shape on A for a wide range of finger shapes other than rectangles. To do this, we adjust the logistical equation such that it is suitable for fitting a plethora of finger cross-sectional shapes:

$$h(x) = h_0\left(\frac{2}{1+(2\,|\,x\,|\,/\,w_0)^a}-1\right) \quad \text{if } h(x) > 0$$
$$h(x) = 0 \qquad\qquad\qquad\qquad\quad \text{if } h(x) \le 0 \tag{1}$$

Examples are shown in Fig. 3. The defining parameters are the obvious width w_0 and height h_0, but also the factor a, which is a measure for the curvature: the higher it is, the closer the shape is to a rectangle. Eq. (1) is suitable for most shapes made with various printing techniques. Even convex shapes with a tip at the top can be fitted with $1 \le a < 2$ (it does not make sense to use $a < 1$ because the maximum h will be smaller than h_0). However, we also add an example in Fig. 3 where Eq. (1) does not fit the measurements well. The reason in that case is slugging of the paste. This is an unwanted effect where a very small portion of A enlarges w significantly. Hence, we may say that Eq. (1) is suitable for the very most finger shapes that are desirable. This narrows down the applicability of Eq. (1) in contrast to the commonly used 'filling factor' F, which is defined as A/w_0h_0. While F is a more general number, Eq. (1) provides a functional description of the finger shape. To convert a to F, you may use the approximation $F = -0.0002a^4 + 0.0051a^3 - 0.0559a^2 + 0.2992a + 0.1542$. Vice versa, you may guess a from F by using $a = 759.87F^4 - 1818.9F^3 + 1637.4F^2 - 647.11F + 95.502$ (the integration of Eq. (1) yields $A = h_0w_0(2H-1)$ with H as hypergeometrical ${}_2F^1$ function [15]; the polynomials are an approximation to $2H-1$ or its inverse).

When investigating variations in A, it is advantageous to fix a certain cross-sectional area as A_0, for example the one observed in a measurement, and to define variations via $A = fA_0$ with a fractional parameter f. The width then depends on A as follows:

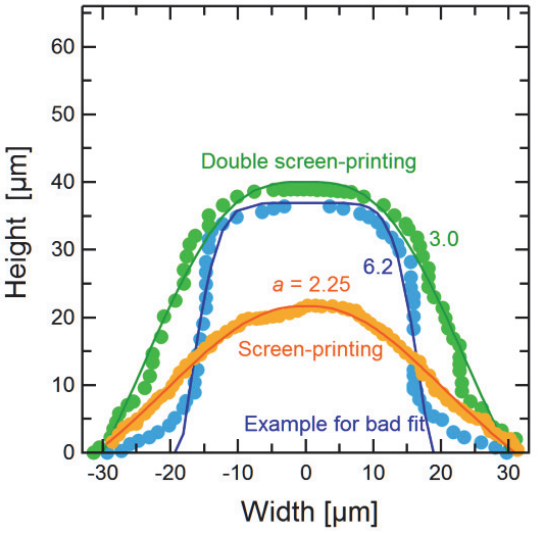

Figure 3. Cross-sectional finger shapes: a screen-printed finger [16] as is typical in present-day manufacturing, a double printed finger [17], and a double printed finger with slugging. The fit function (lines), Eq. (1), fits the measurements (symbols) well except for slugging.

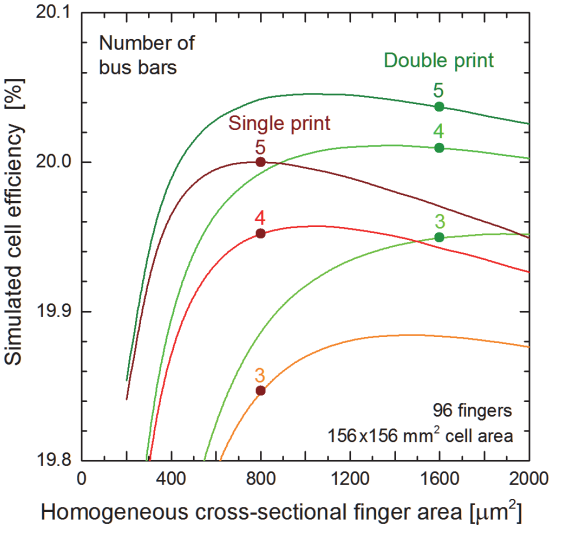

Figure 4. Simulated cell efficiency in dependence of the homogeneous cross-sectional finger area A for the screen-printed finger [16] and the double-printed finger [17] in Fig. 3. The width of the fingers is calculated with Eq. (2).

$$w = \sqrt{\frac{w_{\min}^2}{2^2} + \frac{w_0 - w_{\min}}{h_0} fA_0} + \frac{w_{\min}}{2} \quad (2)$$

In Fig. 3, we choose one shape from Ref. [16] as a typical representative for screen printing in today's mass-production ($w_0 \approx 60$ µm, $h_0 \approx 20$ µm, $A \approx 800$ µm^2, $a = 2.25$). We add another shape from Ref. [17] as an example for double screen-printing having the same with ($w_0 \approx 60$ µm, $h_0 \approx 40$ µm, $A \approx 1600$ µm^2, $a = 3.0$).

Fig. 4 shows the simulated cell efficiency in dependence of A for the screen-printed and the double-printed examples of Fig. 3 (for a start, assuming homogeneous fingers). Towards too small A values, efficiency drops due to resistive losses, towards too high A values, efficiency drops again due to shading. The more busbars there are, the smaller the A with the maximum efficiency because the finger lengths is shorter, and with this the resistive losses. At first sight, one may think that the screen-printed finger is optimum for 5 bus bars and the double-printed finger for 3 bus bars. However, we will see in the next section that A is usually kept smaller than optimum to save silver, and that this can be achieved without considerable loss in efficiency. We will therefore see that the screen-printed finger is optimum only for 3 bus bars and that the double-screen printed finger has a loo large A for all cases. While a large curvature a (obtained with double printing, stencil printing or other techniques) is desirable, more desirable is a small width w_0. Fig. 4 also indicates that having $w_0 = 60$ µm, cell efficiency stays the same when going from 3 to 4 bus bars and from double-printing to single screen-printing.

4. Modeling inhomogeneous fingers

When modeling homogeneous fingers, the IV curve from the device simulation is usually fed into a spice simulation that contains only half a finger, because this is the irreducible simulation domain of the front metallization, as sketched in Fig. 5. It is usually sufficient to discretize half the finger length with about 15 resistors having resistance $R_{s.seg}$ each; any higher number of resistors does not affect the solution significantly anymore (except at unreasonably high resistances). When simulating fingers that are inhomogeneous, however, the whole cell or at least a large part of it needs to be simulated with the SPICE model, and the number of resistors needs to be increased to at least 40 per half finger, so each variation in A does not extend over a too large finger segment. In our simulations, we take 96·40 = 3840 resistors as indicated in Fig. 5. A test simulation using double as many resistors did not yield significantly different results.

A histogram of A-values is transformed to a histogram of $R_{s.seg}$-values, which is then mapped randomly onto all finger segments. Fig. 6 shows a test simulation with a given percentage of failure segments having $A = 10$ µm^2 instead of 800 µm^2 attributed to all other finger segments. The thousand J_{sc}, FF-values in each simulation shown in Fig. 6 scatter because the lumped resistance of the metal grid depends on the positions of each failure segment: if it is situated close to a bus bar, more current flows through the failure segment than if it is situated near the middle between two bus bars and, due to $P = R_{s.seg}I^2$, more power P is dissipated. It is not surprising that if already 1% of segments are failures, the fill factor drops already markedly. By the way, in photoluminescence (PL) or electroluminescence (EL) images of such a cell, parts of the fingers would appear dark.

While *FF* is affected badly, J_{sc} is rather unaffected because the fingers are – apart from the few failure segments – homogeneous. For calculating J_{sc}, the various widths of the segments are accounted for, and the resulting total metallization area of the fingers is multiplied by the optical shading factor f_{opt}. It is well known that f_{opt} is smaller than 100% because part of the light hitting the metal fingers is either directly reflected onto the non-metallized part of the cell (in case of air), or reflected via the front glass interface (if the cell is encapsulated in a module). Tab. 1 lists the measured f_{opt} values of various finger shapes in various surroundings. We choose f_{opt} = 42% for all simulations in this paper.

Table 1. Measured optical shading factor f_{opt} of front metal fingers. Multiplying the metallization area of the fingers with f_{opt} yields the shading.

Technology	Cell surface	Ambient	f_{opt}	Ref.
Plating	Planar/textured	Air	70%	[18]
Aereosol	Textured	Air	72%	[19]
Screen printing	Textured	Air	69%	[19]
Plating	Planar	Module	28%	[20]
Plating	Textured	Module	32%	[20]
Aereosol	Textured	Module	43%	[19]
Screen printing	Textured	Module	42%	[19]
Screen printing	Textured	Module	42-45%	[21]

Screen-printed metal fingers have a usual variation of *A* down to about *A*/2 at locations where screen filaments cross the openings of the screen. For simulating screen-printed fingers, we choose a histogram of *A* containing two values, A_0 and $A_0/2$. Now let us apply such inhomogeneous fingers to a scenario intended for saving silver. The insets in Fig. 7 show the simulated efficiency in dependence of a homogeneous *A* as in Fig, 4, with the variation in *A* as shaded area. The dots indicate the thousand simulated J_{sc} and *FF* values in dependence of *A* for two different A_0 values: one at the optimum A_0 = 800 µm^2, the other two at the sub-optimal A_0 = 600 µm^2. Note that the spread in *FF* is wider with 4 instead of 5 bus bars. However, it is important to note that the extension of each data cloud is about ten times smaller than is commonly observed in mass production, where 50% of J_{sc},*FF*-values lie in a range of about ΔFF = 0.2 and ΔJ_{sc} = 0.2 mA/cm^2. In the simulation, the variation in *FF* is only insignificantly enhanced if the *A*-histogram is filled between A_0 and $A_0/2$. As long as *A* does not vary below $A_0/2$, it implies that the inhomogeneity within each metal finger has a far smaller impact on efficiency spread than the process stability (variations of fingers from cell to cell over long production times) and other variations affecting *FF* and J_{sc} like contact resistivity, front surface passivation etc. [1]. This also means that saving silver by choosing a sub-optimal A_0 causes a rather modest

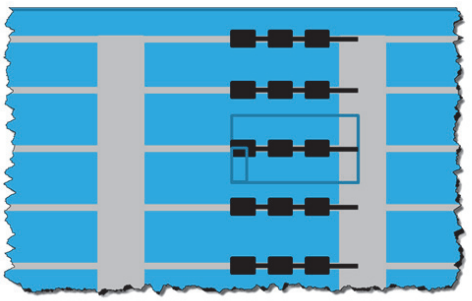

Figure 5. The simulation domain of the three-dimensional device simulation (smallest rectangle), and of the SPICE simulation with homogeneous fingers (larger rectangle). For inhomogeneous fingers, the whole cell must be included into the SPICE simulation. Not drawn to scale.

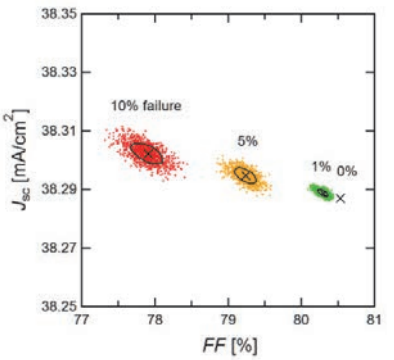

Figure 6. The short-circuit current vs. the fill factor of thousand simulations with the given percentage of failure segments, which have a cross-sectional area *A* = 10 µm^2 instead of 800 µm^2.

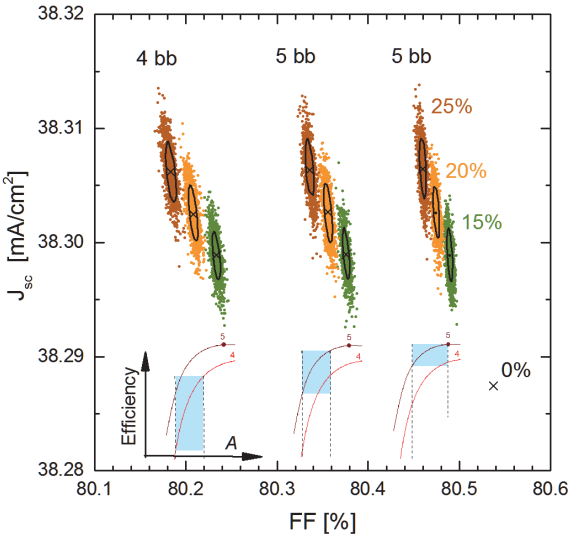

Figure 7. One thousand simulations each of screen-printed fingers whose cross-sectional area A is smaller in the given percentage of segments due to filaments crossing the openings of the screen. Left: a sub-optimal A for saving silver with 4 and 5 bus bars; right: an optimal A with 5 bus bars. The insets show the simulated cell efficiency in dependence of A as in Fig. 4.

additional scattering of fabricated efficiency values. Which suboptimal A_0-value is best depends mainly on the cost of silver and on the minimum tolerable efficiency level. It may be – at times – smaller than 600 μm^2. For a fine example of simulations see Ref. [2].

5. Requirements in near future

The choice of a sub-optimal A_0 needs to be taken into account when predicting targets of A for the near future. The target depends on the number of bus bars, as we saw in Figs. 4 and 7, and on the number of fingers, as we saw in Fig. 1. In standard mass production, improvements in efficiency will necessitate a lower emitter saturation current J_0 which, in turn, implies an increase in its sheet resistivity ρ_{sh} (assuming that the junction depth cannot be made significantly deeper with low-cost approaches). PERL cells that held the world record efficiency for decades [22] had an emitter with ρ_{sh} = 194 Ω/sq due to a deep junction and a finger pitch near 1 mm. If ρ_{sh} were made higher by further lowering the dopant density at the surface, the amount of surface recombination would have started to increase again due to an increase in minority carrier density and a comparable slow decrease in surface recombination velocity. Our simulations show that with shallow junctions as in low-cost approaches, it will still not be necessary in future cell design to increase the number of fingers considerably above about 155 (equivalent to a finger pitch of about 1 mm) when having five bus bars. Even if a multi-bus bar approach is taken, it will still be better to keep the number of fingers limited to near 155 to avoid shading compared to the little savings on resistive losses. Remember from Sec. 2 that the number of fingers will be mostly determined by the emitter and not by other geometries of the metallization. This makes predicting a desirable target for A reliable. Fig. 8 shows the simulated cell efficiency in dependence of A for 155 homogeneous fingers, respectively (for a physical explanation, see discussion of Fig. 4). Remembering from the previous section that finger inhomogeneity has a relatively small impact on cell efficiency, it becomes apparent in Fig. 8 that the target is $A \approx 300$ μm^2 and definitely not far below in case of five bus bars. Having six or seven bus bars would not change this target value significantly, only a multi-bus bar approach would do so.

Finally, let us look at the trends in recent years. Fig. 9 shows our literature collection as filled symbols [16,17,23-34]. We do not aim at completeness, but still a steady trend is apparent, indicated by arrows along the screen printed values and along the double printed values. The red circle indicates the approximate range of present-day screen-printing in mass production. The circled values indicate what is presently possible, as communicated by paste manufactures at the Workshop [35-38]. The three dashed lines indicate circular plating starting from a 5, 10, or 15 µm wide seed finger. In order to make the values achieved with plating directly comparable to screen-printing and other printing techniques, the width of plated fingers is plotted smaller than in reality to account for the smaller f_{opt} of plated fingers, i.e. the width is reduced by the factor f_{opt}(plating)/f_{opt}(screen-printed) = 32%/42% = 0.762 according to Table 1. Furthermore, A of plated fingers is plotted larger than reality to account for the lower metal resistivity of plated fingers compared to screen-printing, i.e. by the factor ρ(plating)/ρ(screen-printing) = 3.5 µΩcm/2.5 µΩcm = 1.4. Note that screen-printing, double printing and stencil printing all move closer towards the three dashed lines representing circular plating. Other printing techniques indicated by various symbols blend in. Thinking of $A \approx 300$ µm^2 as target, device physics (in particular of the emitter) does not give a compelling reason for introducing plating. Hence, it is likely that plating will only be introduced if there is an economic pain for the standard printing techniques, e.g. from a high silver price. Even when thinking of a multi-bus bar approach, homogeneity of the fingers (as achieved with plating) is not a big advantage; even some interrupted fingers per cell will not affect cell efficiency significantly, so the traditional printing techniques may be well suited if they can realize about 30 µm wide fingers. While Ref. [39] predicts that the PERC cell design will be the moving target in mass production for some time to come, our present paper predicts that screen-printing will be the moving target in metallization for some time to come. This is so regardless whether module interconnects stay with about 5 bus bars or change to multi-bus bar designs. Mainly economic pain due to high silver prices may favor a transition to (near) silver-free printing techniques.

6. Conclusions

The model for inhomogeneous front metal fingers developed here can be applied to a wide range of phenomena and can provide a quantitative basis for desirable targets in cell design and for road maps. The model allows us to calculate the sub-optimum cross-sectional area A of front metal fingers to save silver but still to keep the spread of fabricated efficiency values sufficiently tight. A near future target of $A \approx 300$ µm^2 is derived from a combination of both modeling and a literature collection of metallization data. It suggests that screen-printing will be the moving

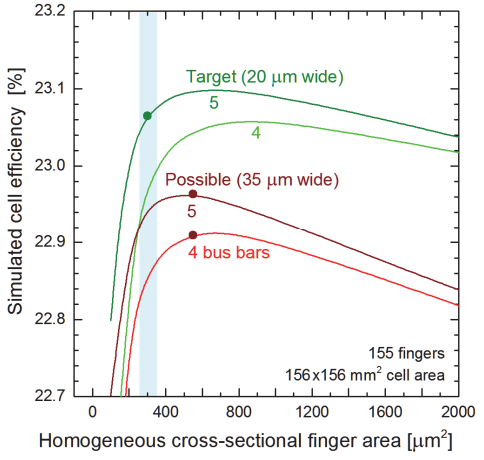

Figure 8. Simulated cell efficiency vs. homogeneous cross-sectional finger area A for the screen-printed finger that is circled in Fig. 9, and for a target finger in near future, indicated by the empty symbol in Fig. 9.

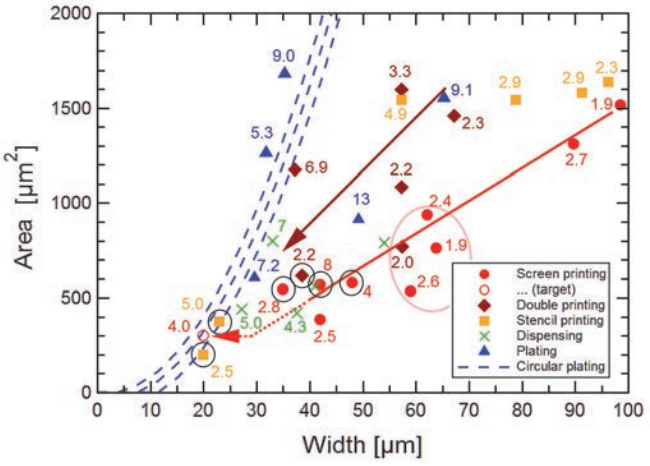

Figure 9. Literature values of recent years [16,17,23-34] of width and cross-sectional area A of metal fingers printed with the indicated printing techniques. The red circle indicates the approximate range of present manufacturing of screen-printed fingers. Circled symbols indicate state-of-the-art values [35-38]. The trends over recent years are indicated by the arrows. The numbers indicate the curvature parameter a in Eq. (1).

target in metallization for some time to come, and mainly economic pain from a high silver price (and not device physics) may favor a transition to (near) silver-free techniques.

References

[1] Müller M, Altermatt PP,Wagner H, Fischer G. Sensitivity analysis of industrial multicrystalline PERC silicon solar cells by means of 3-D device simulation and metamodelling. IEEE Journal of Photovoltaics 2014;4;107-113.
[2] Wong J, Shanmugam V, Cunnusamy J, Zahn M, Zhou A, Yang R, Chen X, Aberle AG, Mueller T. Influence of non-uniform fine lines in silicon solar cell front metal grid design. Prog. PV 2015;23;1877-1883.
[3] Rommel S, Einsele F, Guo H, Ametowobla MF, Manz D. Homogeneity of screen printed metallization lines and relevance for solar cell efficiencies. 26th EU PV Solar Energy Conf. 2011:1538-1541.
[4] Altermatt PP. Models for numerical device simulations of crystalline silicon solar cells – a review. Journal of Computational Electronics 2011; 10: 314-331.
[5] Steinkemper H, Rauer M, Altermatt PP, Heinz FD, Schmiga C, Hermle M. Adapted parameterization of incomplete ionization in aluminum-doped silicon and impact on numerical device simulation. J. Appl. Phys. 2015; 117: 074504.
[6] Richter A, Glunz SW, Werner F, Schmidt J, Cuevas A. Improved quantitative description of Auger recombination in crystalline silicon. Phys. Rev. B 2012; 86: 165202.
[7] International technology roadmap for photovoltaic (ITRPV), Seventh edition, March 2016.
[8] Rousseuuw PJ, Ruts I, Tukey JW. The Bagplot: A Bivariate Boxplot. The American Statistician 1999; 53: 382-387.
[9] The R foundation for statistical compting, 2015, version 3.2.3.
[10] Wolf HP. Package 'aplpack' 2015; University of Bielefeld, Germany.
[11] Greulich J, Fellmeth T, Glatthaar M, Biro D, Rein S. IEEE J. of PV 2012;2: 588-591.
[12] Mette A. New concepts for front side metallization of industrial silicon solar cells. PhD thesis 2007; University of Freiburg, Germany.
[13] Grid Calculator 2016; PVlighthouse, Coledale NSW, Australia.
[14] Fellmeth T, Clement F, Biro D. Analytical modeling of industrial-related silicon solar cells, IEEE J. of PV 2014;4: 504-513.
[15] Mathematica, Wolfram Research.
[16] Pham T, Zhang W, Gou T, Buzby D, Murphy K. Improving electrical performance by double print method and non-contact busbars. 25th EU PV Solar Energy Conf. 2010: 2378-2380.
[17] Hwang MI, Kim SK, Lee K, Moon IS, Lim JK, Lee JC, Kyeong DH, Lee WJ, Cho EC. Fine and high aspect ratio front electrode formation for improving efficiency of multicrystalline silicon solar cells. 25th EU PV Solar Energy Conf. 2010: 1792-1795.
[18] Blakers AW. Shading losses of solar-cell metal grids. J. Appl. Phys. 1992; 71: 5237-5241.
[19] Woehl R, Hörteis M, Glunz SW. Determination of the effective optical width of screen-printed and aerosol-printed and plated fingers. 23rd EU PV Solar Energy Conf. 2008: 1377-1382.
[20] Stuckings MF, Blakers AW. A study of shading and resistive loss from the fingers of encapsulated solar cells. Solar Energy Materials and Solar Cells 1999; 59: 233-242.
[21] Witteck R, Schulte-Huxel H, Holst H, Hinken D, Vogt M, Blankemeyer S,Köntges M, Bothe K, Brendel R. Optimizing the solar cell front side metallization and the cell interconnection for high module power output. Energy Procedia 2016 (to appear).
[22] Altermatt PP, Heiser G, Aberle AG, Wang A, Zhao J, Robinson SJ, Bowden S, Green MA. Spatially resolved analysis and minimization of resistive losses in high-efficiency Si solar cells 1996. Prog. in PV; 4: 399-414.
[23] Mette A, Pysch D, Emanuel G, Erath D, Preu R, Glunz SW. Series resistance characterization of industrial silicon solar cells with screen-printed contacts using hotmelt paste. Prog. Photovolt. 2017;15: 493–505.
[24] Heurtault B, HoornstraJ. Towards industrial application of stencil printing for crystalline silicon solar cells. 25th EU PV Solar Energy Conf. 2010: 1912-1916.
[25] Specht J, Zengerle K, Pospischil M, Erath D, Haunschild J, Clement F, Biro D. High aspect ratio front contacts by single step dispensing of metal pastes. 25th EU PV Solar Energy Conf. 2010: 1867-1870.
[26] Dhamrin M, Nagashima S, Suzuki S, Kamisako K. High conversion efficiency above 18% on non-selective emitter screen-printed crystalline silicon solar cells. 26th EU PV Solar Energy Conf. 2011: 1703-1706.
[27] Magnone P, De Rose D, Zanuccoli M, Tonini D, Galiazzo M, Cellere G, Guo HW, Frei M, Sangiorgi E, Fiegna C. Understanding the impact of double screen-printing on silicon solar cells by 2-D numerical simulations. 37th IEEE PV Specialists Conf. 2011: 2177-2180.
[28] Hoornstra H., Heurtault B. Stencil print applications and progress for crystalline silicon solar cells. 24th EU PV Solar Energy Conf. 2009: 989-992.
[29] Patel K, Yoshioka Y, Baldyga RD, Zhang W. Front side photovoltaics metallization pastes for high aspect ratio grid lines. 37th IEEE PV Specialists Conf. 2011: 1154-1156.
[30] Kossen E, Heurtault, B, Stassen AF. Comparison of two step printing methods for front side metallization. 25th EU PV Solar Energy Conf. 2010: 2099-2010.
[31] Hannebauer H, Falcon T, Hesse R, Dullweber T, Brendel R. 18.9%-efficient screen-printed solar cell applying a print-on-print process. 26th EU PV Solar Energy Conf. 2011: 1607-1610.
[32] Ebong E, Cooper IB, Rounsaville B, Rohatgi A, Dovrat M, Kritchman E, Brusilovsky D, Benichou A. Successful implementation of narrow Ag gridlines with ink jet machine for high quality contacts to silicon solar cells. 26th EU PV Solar Energy Conf. 2011: 1711-1714.

[33] Hoffmann E, Röder TC, Conrad B, Köhler JR, Werner JH. Two step process for optimized laser transferred contacts. 26th EU PV Solar Energy Conf. 2011: 1640-1643.
[34] Pospischil M, Klawitter M, Kuchler M, Jahn M, Efinger R, Schwarz R, Wende L, König M, Clement F, Biro D. High speed dispensing with novel 6“ print head. 6th Metallization Workshop, Konstanz, Germany, 2016.
[35] Cunnusamy J, AMSPT, Singapore. Oral communication at this Metallization Workshop,
[36] Galliazzo M, AMAT, Olmi di S.Biagio di Callalta, Italy. Oral communication at this Metallization Workshop.
[37] Inns DA, DuPont, Sunnyvale, CA, USA. Oral communication at this Metallization Workshop.
[38] Berube G, Heraeus, West Conshohocken, PA, USA. Oral communication at this Metallization Workshop
[39] Min B, Wagner H, Müller M, Neuhaus H, Brendel R, Altermatt PP. Incremental efficiency improvements of mass-produced PERC cells up to 24%, predicted solely with continuous development of existing technologies and wafer materials. 31st EU PV Energy Conf. 2015: 473-476.